76

CHARACTERIZATION OF THE DRYLINE IN ALBERTA: OBSERVATIONS FROM UNSTABLE 2008

Neil M. Taylor[1*], David M. L. Sills[2], John M. Hanesiak[3], Craig D. Smith[4], and Julian C. Brimelow[1]

[1]National Lab-West, Environment and Climate Change Canada (ECCC), Edmonton, AB
[2]Science and Technology Branch, ECCC, King City, ON
[3]Centre for Earth Observation Science, University of Manitoba, Winnipeg, MB
[4]Climate Processes Section, ECCC, Saskatoon, SK

1. INTRODUCTION

In the summer of 2008, Environment and Climate Change Canada (ECCC; formerly Environment Canada) scientists partnered with colleagues in academia to lead a field study investigating thunderstorm initiation (TI) in the foothills region of Alberta. The Understanding Severe Thunderstorms and Alberta Boundary Layers Experiment (UNSTABLE; Taylor et al. 2011) intensive observation period (IOP) was conducted during 9-23 July 2008. During this time fixed and mobile observation platforms were used to examine near-surface and upper-air processes related to TI.

One goal of the campaign was to improve our understanding of the dryline and the role it may play in TI. A first step in this regard is to quantify thermodynamic and kinematic contrasts across the dryline in the context of stability and TI. The rationale is to provide forecasters and researchers with an appropriate conceptual model to associate with the dryline in this region. Subsequently, forecasters are better equipped to anticipate dryline development, recognize its presence/evolution in synoptic-scale observation networks, and consider influences on (severe) thunderstorm forecast and alerting decisions. To this end, observations of the dryline obtained during UNSTABLE are treated here collectively. While based on a small sample size, features consistent among multiple drylines bring us a step closer to formalizing a conceptual model for the dryline in Alberta.

2. DATA AND ANALYSIS TECHNIQUES

The study area and instrumentation referenced herein appear in Fig. 1. The red polygons highlight the study domains; an inner domain designed to focus on observations of mesoscale boundaries and TI, and an outer domain focused on storm and boundary evolution. Typical dryline distances from radars in Alberta preclude their identification via reflectivity fine lines. Dryline identification using visible satellite imagery is also challenging as the boundary is frequently not associated with a line of developing cumulus clouds. As such, a mesoscale network of surface observations was critical for dryline identification. The surface network was augmented with other fixed and mobile instrumentation to provide both near-ground and upper-air observations in the vicinity of the dryline (see Table 3 in Taylor et al. 2011 for details).

2.1 *Fixed Surface Observations*

Surface observation networks consisted of operational hourly surface stations, the University of Calgary Foothills Climate Array (FCA), and seven mesonet stations installed by ECCC. The result was a combination of hourly and one-minute observations. Mesoanalyses were produced for each hour that boundaries were observed and one-minute observations provided additional details on their passage and evolution. Drylines were primarily identified via pairs of surface observations on either side of surface boundaries that were not associated with fronts, storm outflow or other boundaries. We followed the criterion used by Hoch and Markowski (2005) requiring a gradient in water vapour mixing ratio (q_v) between paired stations of at least 3 g kg^{-1} 100 km^{-1} (0.03 g kg^{-1} km^{-1}). Where pressure data were not available (e.g., hourly FCA stations), a gradient criterion in dew point (T_d) of 0.08 °C km^{-1} was used. The above criteria defined a dryline if paired observations along its length met or exceeded the gradient thresholds. In a small number of cases, where paired observations fell slightly below the criteria but adjacent pairs along the dryline in both along-line directions met the criteria, the sub-criteria observations were used. This situation occurred in only 1% (2%) of paired T_d (q_v) observations. Note that sub-criteria observation pairs were not used in the analysis of section 4 below.

* *Corresponding author address:* Neil M. Taylor, National Lab-West, Environment and Climate Change Canada. 9250-49th Street Edmonton, AB, T6B 1K5; Email: neil.taylor@canada.ca

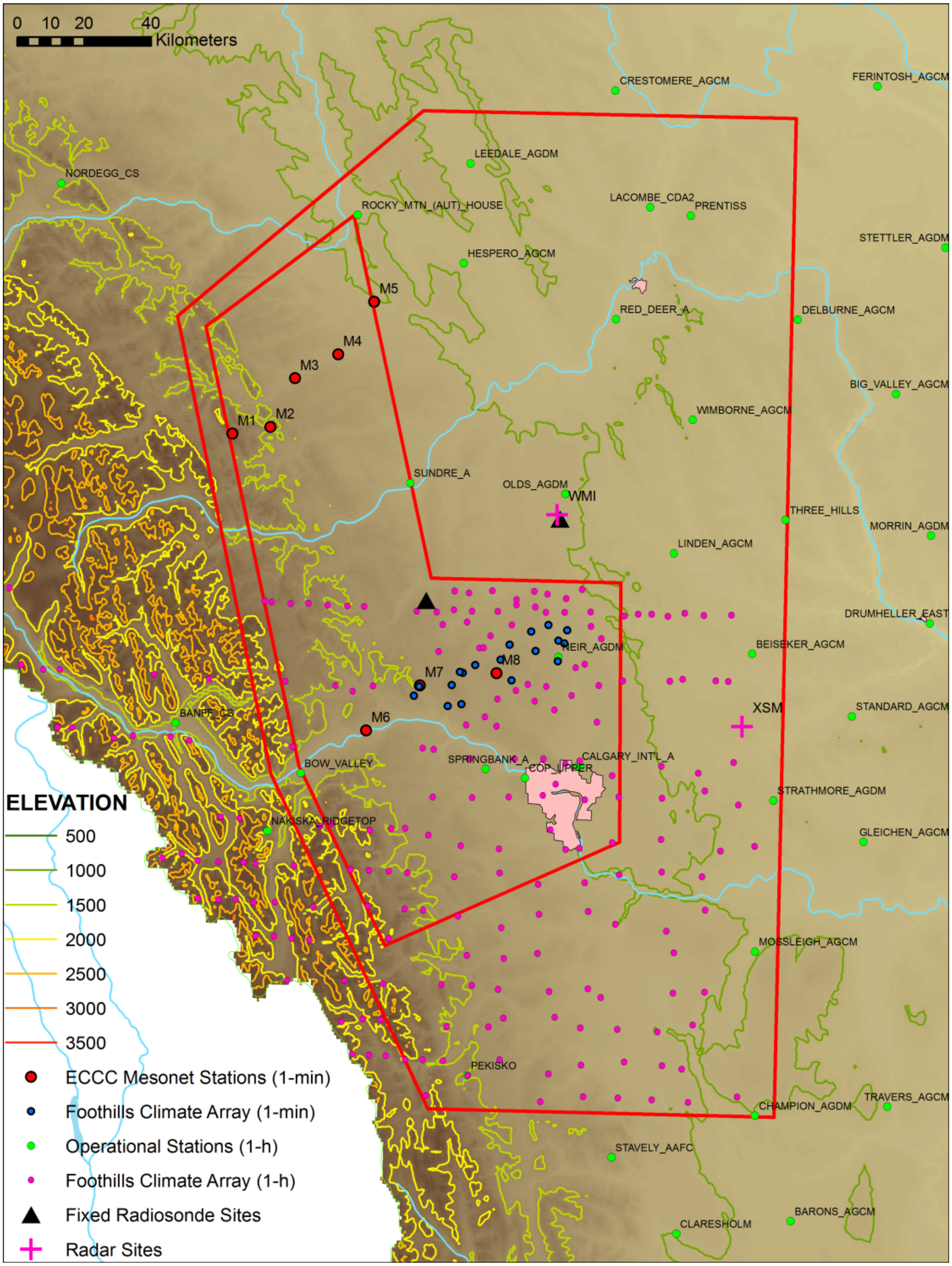

Fig. 1: Map of instrumentation locations used for the present analysis. The UNSTABLE study domains are indicated by red polygons. Elevation contours are as indicated in meters above sea level. Hourly and one-minute surface station networks and fixed radiosonde sites are as indicated with details found in Taylor et al. (2011). Locations of mobile surface and upper-air teams are not shown. The radar sites are indicated for the Weather Modification Inc. (WMI) and ECCC Strathmore (XSM) radars.

2.2 *Mobile Surface Observations*

Up to three mobile surface stations were used to sample boundaries and other phenomena during UNSTABLE. The primary station was the Automated Mobile Meteorological Observation System (AMMOS; Fig. 2) which collected 2-s observations of temperature (T), T_d, wind (at ~3 m), and pressure (P). The other mobile stations collected 2-s or 15-s observations of T, T_d, and P but the slower response time of their sensors limited use of the resulting data to hourly mesoanalysis applications only.

For mesoscale boundary analysis, the AMMOS conducted repeated transects across boundaries with extended time on either side of the boundary to sample near-boundary air. Initial transects were at higher speed (i.e., > 20 km h^{-1}) to locate the boundary with subsequent transects at lower speed (i.e., < 10 km h^{-1}) to obtain more detailed observations.

Fig. 2: The AMMOS mobile surface station.

2.3 *Upper-Air Observations*

Upper-air observations included in the present analysis consist of radiosondes released from two fixed (Fig. 1) and two mobile locations. Locations for mobile upper-air teams were determined from the morning analysis and expected evolution of mesoscale boundaries or other phenomena to be sampled that day. For dryline missions, mobile teams attempted to simultaneously release soundings within 40 km of the dryline and on either side of it to allow for direct comparison of the above-ground, near-dryline environment. Soundings were released every two hours from all four locations on operational days for the period 1200-0000 UTC (0600-1800 LT) at fixed sites and 1600-0000 UTC at mobile sites.

2.4 *Aircraft Observations*

While dedicated instrumented aircraft observations were not available for UNSTABLE, we were able to partner with Weather Modification Inc. (WMI) to obtain targeted observations outside of their hail-suppression operational program. Research flights were conducted opportunistically with 1-s T, T_d, and P data available via an Aventech Aircraft-Integrated Meteorological Measurement System (AIMMS). Aircraft flight plans on dryline missions consisted of ascending/descending spirals on either side of the dryline and stepped traverses across the dryline at altitudes ranging from a few hundred to ~1500 m above ground.

3. ANALYZED DRYLINE POSITIONS

Based on the procedure described in 2.1, we identified 154 unique hourly dryline positions from nine operational days (Table 1). Analyzed positions of all the drylines identified are shown in Fig. 3. Based on the initial analyzed positions on each day, drylines were observed to form very close to the Rocky Mountains in most cases between 1300 and 1600 UTC. Drylines were observed to advance away from higher elevation terrain during the transition from late morning to afternoon as the convective boundary layer (CBL), especially in the dry air, deepened. However, in most areas, dryline progression remained limited to regions above ~1500 m ASL. In some cases, the dryline was seen to advance further to the east (downslope) such as in the northern regions of the UNSTABLE domain and in extreme southern Alberta outside of the study domain. In these cases surface wind observations in the dry air were nearly uniformly downslope and stronger than the wind in the moist air.

Table 1: Days and start-end times (UTC) when drylines were observed.

Day (July 2008)	Dryline Analysis (UTC)
9	15-05
12	14-06
13	14-05
14	14-05
16	16-03
17	13-04
19	14-08
20	14-11
21	12-07

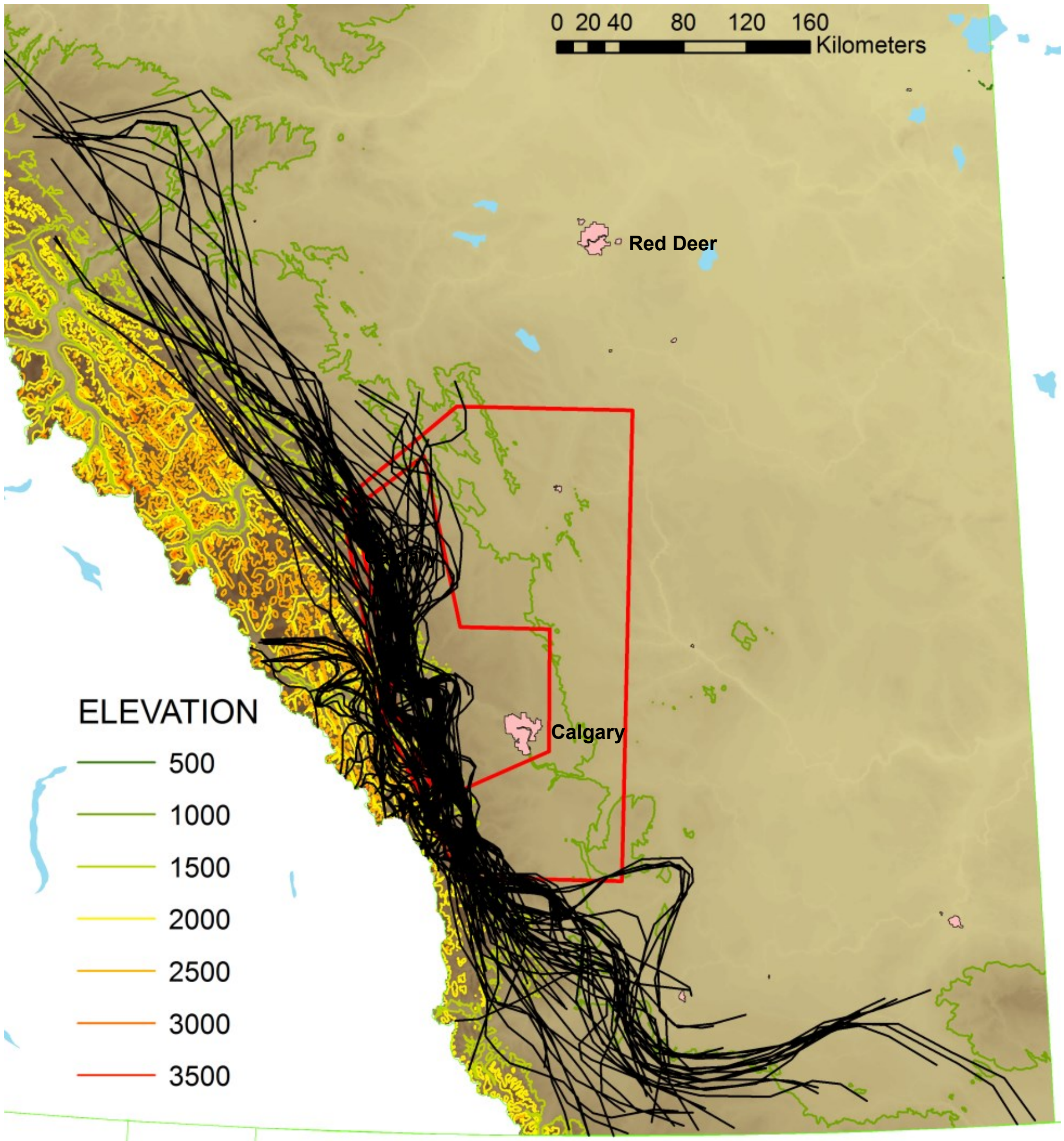

Fig. 3: Analyzed positions of the dryline for the times in Table 1. Red polygons identify the UNSTABLE study area. Elevation as in Fig. 1 and select larger cities are noted.

4. ACROSS-DRYLINE DIFFERENCES

The dryline positions shown in Fig. 3 were obtained via 1234 pairs of surface observations across the dryline. We can examine these data from all analysis times as a whole. Beginning with contrasts in T and T_d (Fig. 4) we see a tendency for small contrasts in T across the dryline but significant differences in T_d with mean (median) values of 2.1 °C (2.3 °C) in the dry air and 7.9 °C (7.7 °C) in the moist air. A subset of observation pairs with pressure data available (174 pairs) can be used to contrast corresponding potential temperature (θ) and q_v. Mean (median) values of θ are 306.8 K (307.0 K) in the dry air and 305.0 K (305.2 K) in the moist air. For q_v, the values are 5.4 g kg^{-1} (5.4 g kg^{-1}) in the dry air and 7.9 g kg^{-1} (7.8 g kg^{-1}) in the moist air.

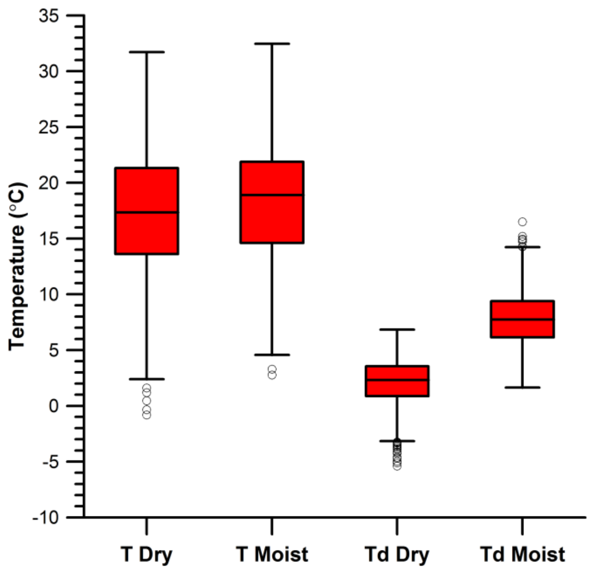

Fig. 4: Boxplots of T and T_d on the moist and dry sides of the dryline via 1234 pairs of fixed observations. Whiskers extend to 1.5x the interquartile range and outliers are indicated by circles.

Several studies have discussed the dryline in terms of a solenoidal circulation (e.g., Sun and Ogura 1979; Sun 1987; Ziegler et al. 1995; Weiss and Bluestein 2002; Weiss et al. 2006) and/or density current (e.g., Bluestein et al. 1990; Parsons et al. 1991; Ziegler and Hane 1993; Hane et al. 1997; Bluestein and Crawford 1997; Atkins et al. 1998; Ziegler and Rasmussen 1998). To consider observations from UNSTABLE in this context we can examine contrasting values of virtual potential temperature (θ_v) and air density (Fig. 5). We find little difference in the distributions of values for the dry and moist air with perhaps a small tendency for the moist air to be characterized by lower (higher) values of θ_v (density).

To examine how dryline strength may vary throughout the day we can examine the evolution of the gradients of q_v and θ_v (Fig 6). We use a similar definition of intensity as in Schultz et al. (2007) though we use the gradient in q_v instead of their difference in T_d. Given the small sample size of observations for each hour we plot mean values only. Differences used for the gradient calculations are based on subtracting values in the dry air from those in the moist air. The plot shows an increase in q_v gradient throughout the day peaking at 0100 UTC (1900 LT) suggesting the dryline 'strengthens' with surface heating and CBL mixing. The mean gradients in θ_v are small but negative after 1600 UTC (1000 LT) suggesting a density contrast across the dryline and consistency with modulation of the density gradient via a solenoidal circulation.

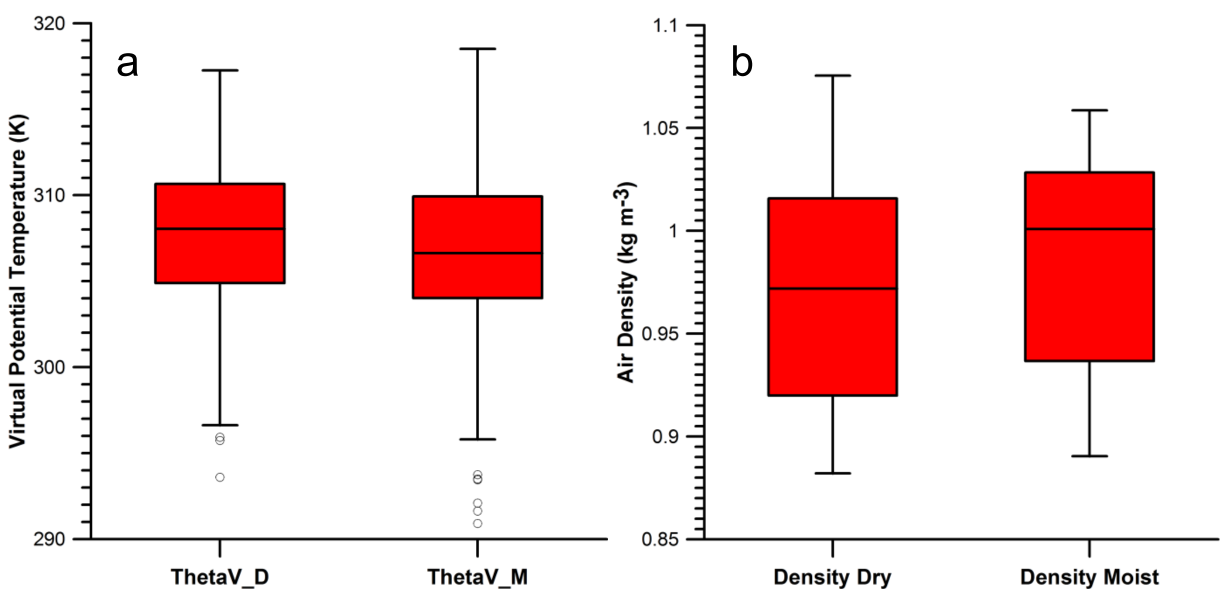

Fig. 5: Boxplots as in Fig 4 but for (a) virtual potential temperature (θ_v; VirPotTempt) and (b) air density (kg m^{-3}) for the fixed observation pairs where pressure data were available.

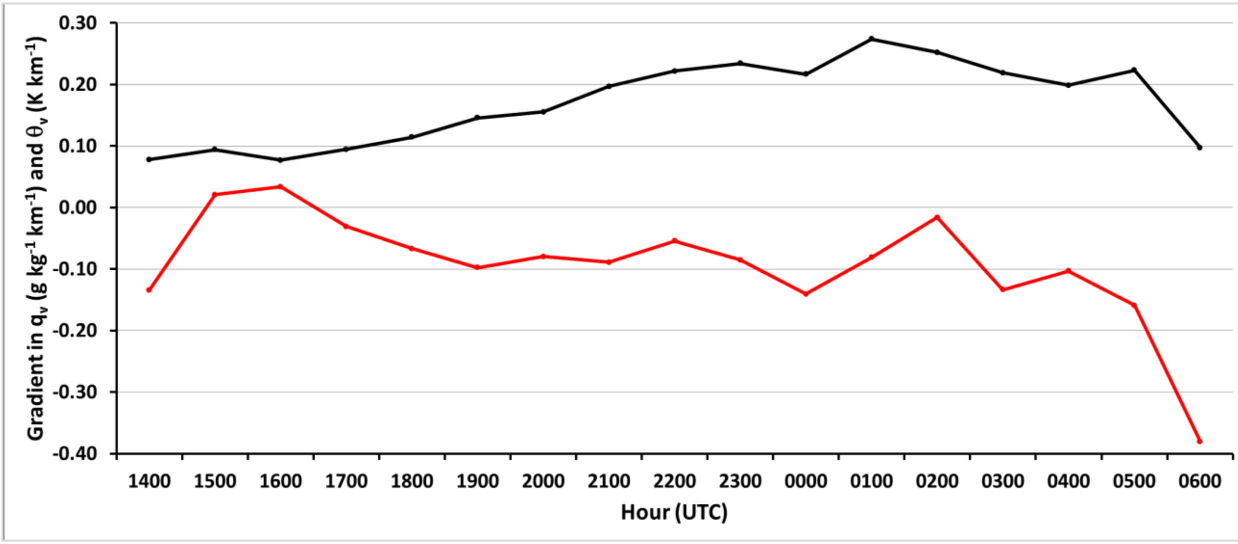

Fig. 6: Hourly mean gradients in q_v (black) and θ_v (red) between fixed observations stations from 1400 UTC (0800 LT) to 0600 UTC (0000 LT). Gradients are calculated by subtracting the values on the dry side of the dryline from those on the moist side.

Only a subset (191 of 1234) of all the paired surface observation stations used included wind observations. As such, the observation density was not sufficient to calculate two-dimensional fields (e.g., divergence) from observations alone. However, we can still assess the general character of the wind in the dry and moist air from the paired observations (Fig. 7).

Wind observations in the dry air (Fig. 7) clearly indicate a preferred west-southwesterly wind direction with a tendency for higher wind speed values than in the moist air. Direction in the moist air appears to be more variable with wind speed less than 8 m s^{-1}. Observations were not further stratified into cases when there was a westerly component to the wind in both the dry and moist air.

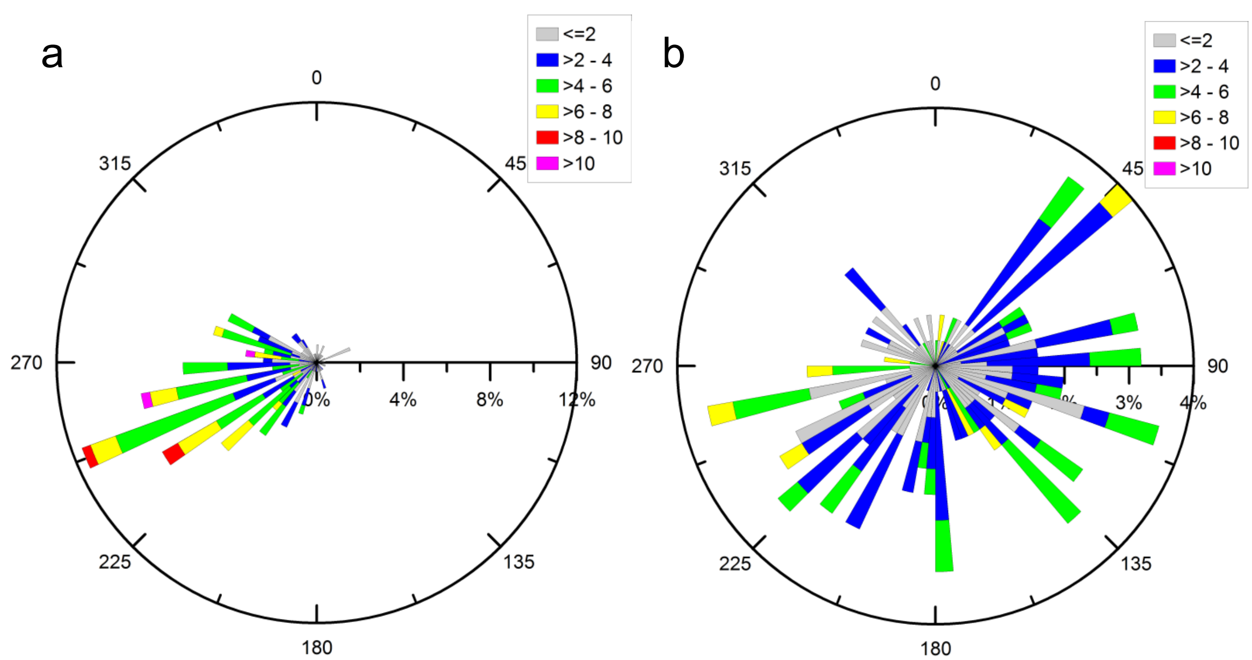

Fig. 7: Wind observations as polar plots from fixed paired observations for (a) the dry side of the dryline and (b) moist side. Wind speed is in m s^{-1} with colours indicated at upper-right for each plot.

Association of the dryline with TI implicitly assumes some correspondence between the dryline and low-level convergence. As a proxy for convergence we apply the definition of confluence used by Schultz et al. (2007). That is, we calculate the difference in the u-component of the wind from observations on either side of the dryline ($u_{dry} - u_{moist}$) so that positive values infer convergence (Fig. 8). Only a small fraction (11 %) of paired wind observations are not associated with positive confluence with the majority of confluence values in the 1-5 m s^{-1} range[†].

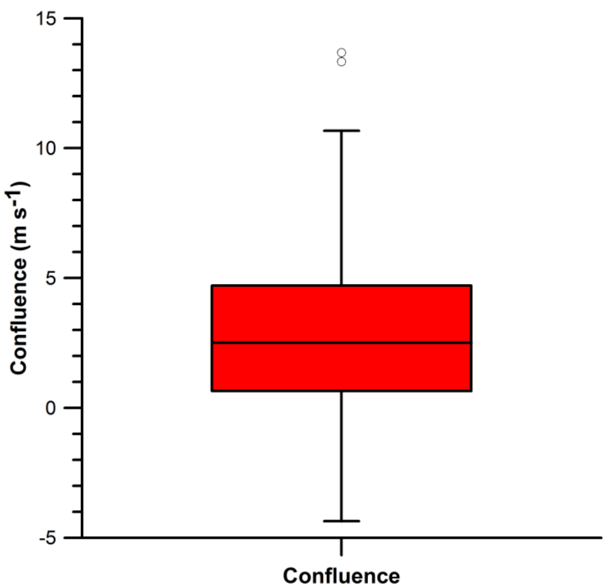

Fig. 8: Boxplot as in Fig. 4 but for confluence as described in the text.

5. DRYLINE BOUNDARY OBSERVATIONS

Using the AMMOS system we obtained 11 detailed cross-dryline transects from four separate days. The level of detail found within each transect through the boundary appeared to vary with time of day and orientation of the vehicle path relative to the boundary. Examples of transects from 13 July 2008 are plotted in Fig. 9 for two distinct segments of road. The first segment (Fig. 9a) was oriented at an obtuse angle to the dryline while the second (Fig. 9b) was oriented more normal to the boundary. The resulting plots show significant variability in q_v over the first road segment (also sampled at earlier times) while the more normal transects (at later times) result in a smoother transition from dry to moist air across the dryline. Further investigation into the source of variability in q_v (and other quantities) across the dryline is required. For example, it is unclear if the minimum in q_v at ~1 km on the 204730-204916 transect may be associated with a transient misocyclone (Ziegler 2016; personal communication).

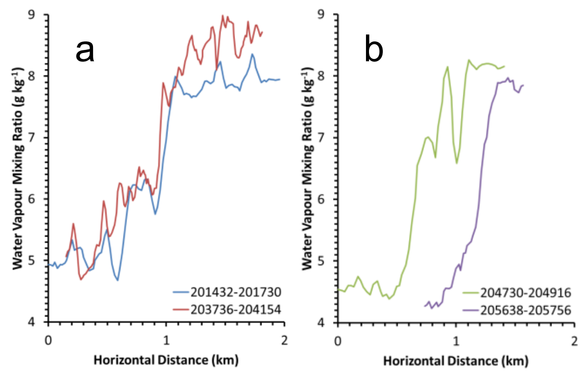

Fig. 9: AMMOS traces of q_v every 2 s across the dryline on 13 July 2008 for (a) a road segment at an angle to the dryline and (b) a road more normal to the dryline. Distances are relative to the westernmost data point in the dry air. Curves identified as HHMMSS in UTC.

Based on endpoints subjectively determined as the maximum and minimum values of q_v associated with the overall dryline gradient, mean differences and gradients of thermodynamic quantities across the dryline are given in Table 2.

Table 2: Mean differences and gradients of various parameters across the dryline via AMMOS observations.

Variable	Difference	Gradient
Temperature	-0.2 °C	-0.2 °C km^{-1}
Dewpoint	7.2 °C	12.0 °C km^{-1}
Mixing Ratio	2.9 g kg^{-1}	4.9 g kg^{-1} km^{-1}
Potential Temperature	-0.2 K	-0.1 K km^{-1}
Virtual Pot. Temperature	0.4 K	0.8 K km^{-1}
Density	1.2 x10^{-3} kg m^{-3}	3.1 x10^{-3} kg m^{-3} km^{-1}
Estimated Width	790 m	

6. NEAR-DRYLINE ENVIRONMENT

Thus far our results have focused on surface-based contrasts between the dry and moist air. Of great interest from a forecasting perspective is the character of the environment above the surface. As discussed in 2.3, simultaneous soundings were obtained on either side of the dryline when

[†] Note that for the present study we have limited our analysis to a conceptual context. More research is required to formalize the link between confluence at the dryline in Alberta and TI.

possible. The result is a set of 12 (34) soundings on the dry (moist) side of the dryline within 40 km of the boundary location from all data available between 1200 UTC and 0000 UTC. Composite soundings were created by first interpolating these profiles to common 5-m increments in height above ground. Mean values of T, T_d, and wind (direction and speed) were then calculated at each level to produce the profiles in Fig. 10.

Here the composite dry profile is characterized by a deep, well-mixed CBL over the lowest 2 km or so with surface T (T_d) of 22 (4) °C and wind from the south-southwest at low levels veering to westerly at the top of the CBL and above. In contrast, the composite moist profile exhibits a CBL only ~1 km deep with T (T_d) of 20 (9) °C and low-level wind from the southeast veering to westerly above the CBL. Of particular interest is the presence of an elevated residual layer (ERL) 'capping' the moist CBL. Note that in both composites a superadiabatic thermal layer and skin layer of moisture are present. It is possible that these are due, at least in part, to the use of surface weather stations as the source of the lowest value in the profile.

For each individual sounding the depth of the superadiabatic layer, CBL, and ERL have been subjectively determined based on values of θ and q_v. The mean values of each are illustrated in Fig 11. Both dry and moist soundings exhibited a superadiabatic layer of ~30 m. For the dry soundings the mean CBL depth was 1980 m with an ERL above of 880 m. The moist soundings have a mean CBL depth of 1040 m and ERL of 870 m. Note the combined depth of the moist CBL and ERL is 1910 m; nearly the same as the CBL depth in the dry air. In looking at mean values of θ and q_v in each layer, there is little change from the surface to the ERL in the dry air with θ ~307 K. In the moist air the CBL is ~1 K cooler than in the superadiabatic layer while the ERL is warmer than both with an average θ ~308 K. In terms of q_v, for the dry air there is a mean ~30-m skin layer with q_v ~5 g kg^{-1} and a mean q_v in the CBL of just under 5 g kg^{-1}. In the cases with an ERL in the dry air, mean q_v is ~4 g kg^{-1}. In the moist air the mean near-surface q_v is ~8 g kg^{-1} with ~7 g kg^{-1} in the CBL. The mean q_v in the moist-side ERL is ~4 g kg^{-1} corresponding with the value in the dry CBL.

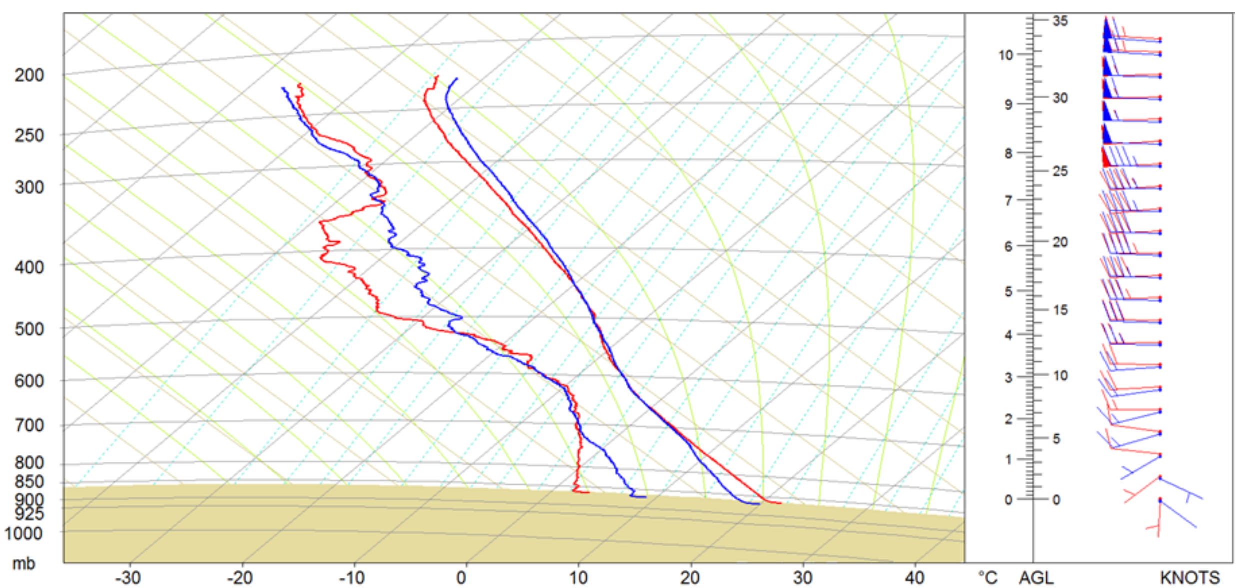

Fig. 10: Composite sounding data (mean values every 5 m in the vertical) for 12 dry (red) and 34 moist (blue) soundings within 40 km of the dryline.

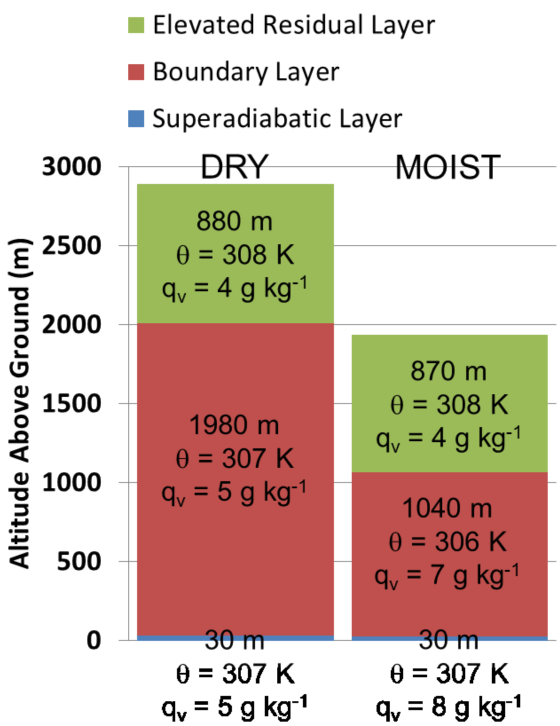

Fig. 11: Mean depth (m) of θ (K) and q_v (g kg^{-1}) for various layers from the sounding dataset used in Fig. 10. Bottom-most values apply to the shallow superadiabatic layer in both the moist and dry soundings.

The composite soundings and layer analysis for the dry and moist air have implications for TI as shown in Table 3. Here we have calculated mean values of 50-mb mean-layer (ML) parcel Lifting Condensation Level (MLLCL), MLCAPE, Convective Inhibition (MLCIN), and total-column Precipitable Water (PW) from all the soundings. The dry air environment is characterized by larger values of MLLCL and smaller values of MLCAPE, MLCIN, and PW than in the moist air environment. Note that individual soundings on the moist side of the dryline, especially in late afternoon, had MLCAPE values much larger than the mean value shown in Table 3 which includes morning soundings.

Table 3: Mean values for selected parameters from the dry and moist soundings described in the text. ML calculations use a 50-mb mixed parcel.

Parameter	Dry	Moist
MLLCL	2535 m	1893 m
MLCAPE	43 J kg^{-1}	278 J kg^{-1}
MLCIN	-15 J kg^{-1}	-31 J kg^{-1}
PW	13 mm	16 mm

Conceptually, in the dry air, this suggests little inhibition of high-based convective cloud development but with potentially significant sub-cloud entrainment and small CAPE limiting updraft strength. Conversely, in the moist air we would expect clouds with lower bases and stronger updrafts but with development modulated by a requirement to overcome more CIN.

A two-dimensional visualization of the dryline boundary and corresponding environment in the dry and moist air is illustrated via aircraft-data cross sections from 13 July 2008 (Fig. 12). In this case we see stratification of θ in both the horizontal (at the dryline) and in the vertical corresponding to the top of the cool, moist CBL to the east of the dryline. A cross-section of q_v shows the striking moisture gradient at the dryline (at distance ~2 km) with the boundary sloping into the moist air with height. While less evident in q_v than in θ, the top of the CBL in this case is ~2.3 km ASL (1.3 km AGL). In both cross-sections, at distances of ~3, 11, 16, and 25 km we see evidence of warm, dry air near the top of the CBL. We suspect these are associated with gravity waves generated near the dryline updraft and propagating downstream of the boundary as vertical motion is constrained by the ERL atop the moist CBL.

7. DISCUSSION AND CONCEPTUAL MODEL

For the present study we have collectively examined observations of the dryline from UNSTABLE in an attempt to refine and 'regionalize' the dryline conceptual model for Alberta. While we recognize the present analysis includes a small number of drylines, it is hoped that by doing so we can help ECCC forecasters appreciate the structure and intensity of the dryline and quantify various characteristics associated with it.

Analyzed dryline positions during the project suggest that dryline genesis likely occurs in close proximity to the steep terrain of the Rocky Mountains by late morning (1000 LT). While we observed a tendency for the dryline to advance downslope in the afternoon, progression in many areas was limited. One area where dryline advancement occurred more frequently was extreme southern Alberta. Observations of stronger wind in the dry air in these cases suggest that this dryline 'bulging' is due to mixing of higher-momentum air from aloft to the surface as has been noted in other studies. Following the terminology of Hane (2004), these cases appear to be synoptically active drylines where larger-scale forcing contributes to the downward transport of momentum to the surface. While these types of drylines did not frequently occur during UNSTABLE, bulging drylines have been previously documented in Alberta (e.g., Knott and Taylor 2000; Dupilka 2004) and been observed by the lead author through unpublished research and operational forecasting experience. Moreover, in some cases portions of the dryline can advance as far as the Saskatchewan border (see Fig 13).

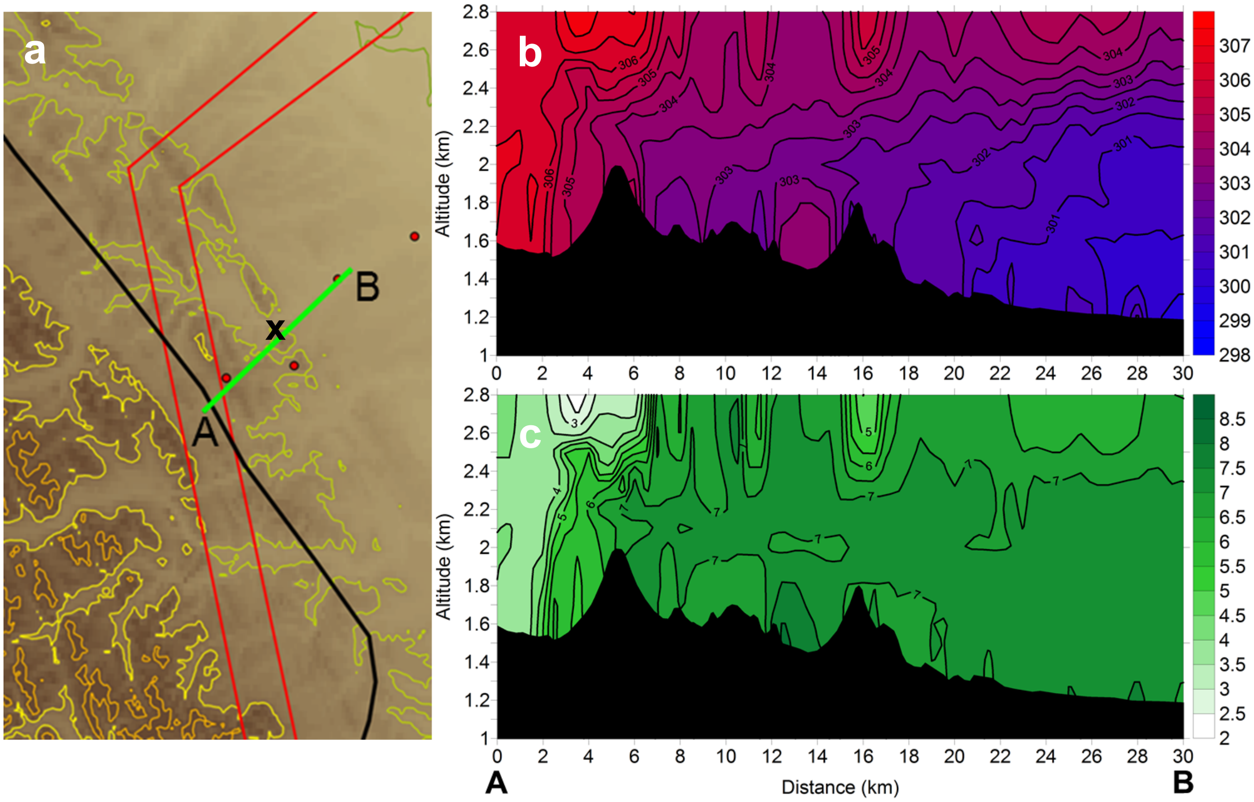

Fig. 12: (a) Map showing the position of the dryline at 1900 UTC 13 July 2008 and the horizontal axis used for the plots at right. Red circles are the mesonet stations identified in Fig. 1 and the location of the sounding used in the analysis is identified with an x. The plots at right show cross-sections of (b) θ (K) and (c) q_v (g kg^{-1}) obtained via aircraft, sounding, and surface observations from 1755-1930 UTC 13 July 2008.

From paired surface observations on either side of the dryline we are able to quantify some thermodynamic and kinematic differences across it. While observed thermal contrasts were small, mean differences in T_d and q_v are 5.9 °C (2.5 g kg^{-1}) for all observed times. These differences correspond to gradients in T_d and q_v of 0.6 °C km^{-1} and 0.2 g kg^{-1} km^{-1}, respectively. Wind in the dry air was observed to be predominantly from the west or southwest with higher speed values than the more directionally variable and weaker wind in the moist air. We found 89% of paired wind observations were associated with positive confluence (mean value 3.0 m s^{-1} for all observations). Mobile surface observations revealed fine-scale structure of the dryline boundary and gradients in moisture variables larger than those of the fixed station analysis. Mean gradients in T_d and q_v were 12 °C km^{-1} and 5 g kg^{-1} km^{-1}, respectively, and consistent with the results of studies in the U.S. (e.g., Pietrycha and Rasmussen 2004; Buban et al. 2007).

Upper-air soundings and aircraft observations provide a clear illustration of the structure of the near-dryline environment and vertical structure of the boundary/circulation. As in other observational and numerical studies, our observations describe a deep, dry, stable environment on the dry side of the boundary and a shallower, cool, unstable environment on the moist side. The moist CBL is capped by an ERL originating in the dry air resulting in increased CIN as compared to the dry environment. Even when considering MLCAPE

values from several soundings at all observation times we find markedly higher CAPE values on the moist side of the dryline highlighting an environment supportive of deep moist convection.
Though we recognize the limitations due to the small sample size, the above results allow us to refine the existing conceptual model for the dryline in Alberta and quantify various characteristics. In Fig. 13 we show a plan-view map characterizing observed dryline locations.

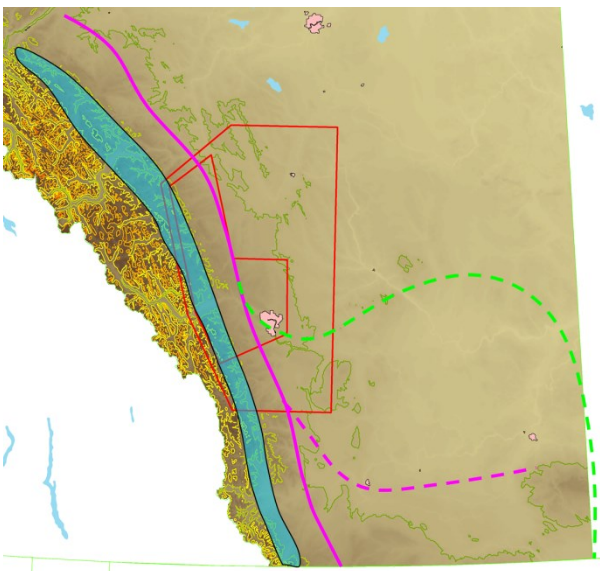

Fig. 13: Plan-view map highlighting the genesis region (shaded blue), maximum eastward extend of quiescent drylines (solid magenta line), and synoptically active drylines (dashed magenta line) during the UNSTABLE 2008 campaign. The green dashed line represents the approximate maximum extent of synoptically active drylines that have been observed in other studies.

Based on analyzed dryline positions before 1600 UTC (1000 LT) we have identified a genesis region that lies in close proximity to the Rocky Mountains. It is premature to conclude what physical mechanism is responsible for initial dryline development here. More observed cases and examination via km-scale NWP simulations may be required to describe the physical processes involved. Quiescent drylines were observed to advance eastward an estimated 40-60 km from the genesis region and remain roughly parallel to the slope of the terrain. In the few cases of synoptically active drylines, the dry air in southernmost Alberta advected to the east so that the dryline boundary becomes oriented in a zonal fashion. More extreme cases of bulging synoptically active drylines have been identified in Knott and Taylor (2000), Dupilka (2004), and in unpublished work by the lead author. We have estimated the extent based on several cases in Fig. 13 for the purposes of illustration and explanation that only a small subset of these types of drylines were observed during UNSTABLE.

A conceptual cross-section was developed by Ziegler and Rasmussen (1998) based on results from three dryline case studies in the U.S. We use their illustration as a starting point to quantify characteristics of the dryline in Alberta (Fig. 14). Based on sounding, aircraft, and mobile surface observations from our limited dataset, the general features of the dryline in Alberta are consistent with the conventional conceptual model. We see a dry CBL ~2 km deep to the west of the dryline and a ~1 km deep moist CBL to the east. A residual layer from the dry CBL is advected over top of the moist CBL and provides mid-level instability for potential TI. The combined depth of the moist CBL and ERL above is approximately the same as the dry CBL to the west. The dryline was observed to vary in width with a mean width ~0.8 km and some fine-scale structure observed within the boundary itself.

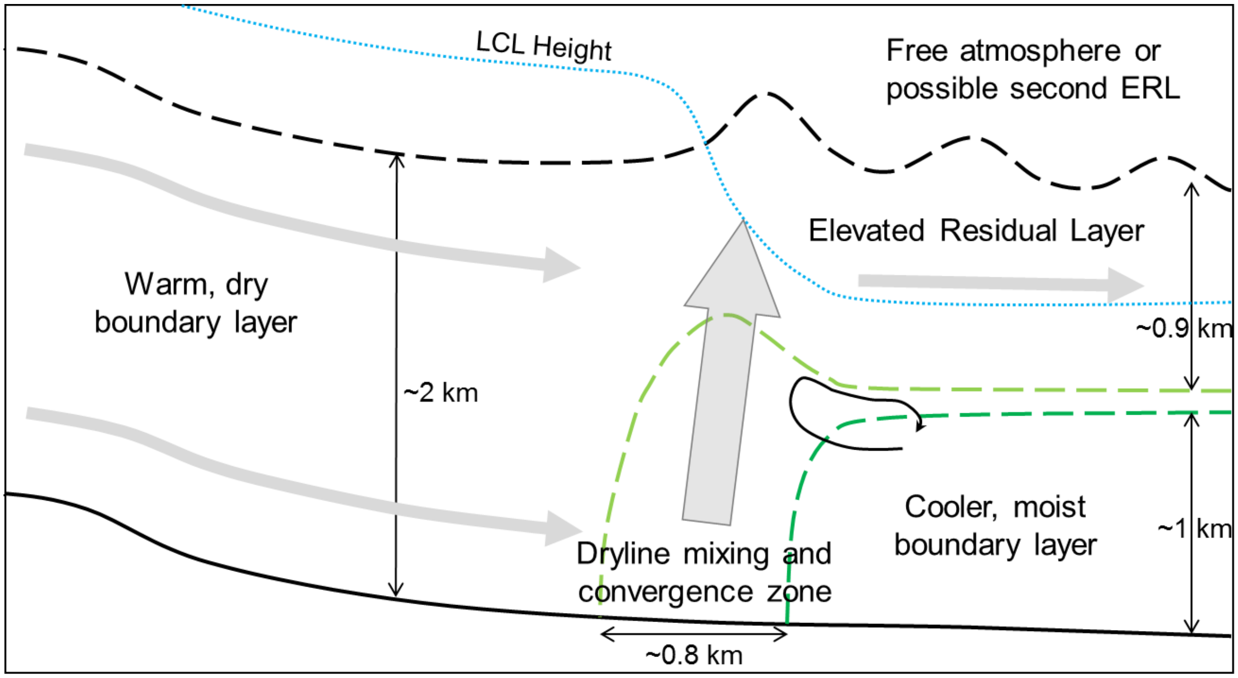

Fig. 14: Cross-section conceptual model adapted from Ziegler and Rasmussen (1998) with values obtained from the present study.

Of particular interest from both a scientific and forecasting perspective is the potential link between the dryline in Alberta and TI. From our observations of a limited number of cases we can draw a few reasonable conclusions with respect to this link (Table 4).

In Table 4 we contrast various characteristics across the dryline. With the exception of the vertical wind shear comparison[‡], this information, coupled with a tendency for the dryline to be associated with confluence (inferring convergence), are consistent with the dryline acting as a mechanism for TI in Alberta. Moreover, stronger CIN on the moist side of the dryline should limit widespread TI and allow discrete convection to realize local latent energy. In addition, a frequent upslope component to the wind in the CBL on the moist side may contribute to stronger deep-layer vertical wind shear though we have not quantified this in the present study. These last two characteristics suggest that the dryline in Alberta provides not only a mechanism for TI to occur but, assuming sufficient instability and deep-layer wind shear are present, could contribute to an environment favourable for the development of severe thunderstorms.

Table 4: Summary of characteristics associated with the dry and moist side of the dryline in Alberta.

Dry Side	Moist Side
Dry and very deep CBL favours significant dilution of ascending parcels	Shallower moist CBL limits dilution of ascending parcels
High LCL and LFC heights due to warm near-surface temperatures and low dew point values	Much lower LCL and LFC heights due to slightly cooler near-surface temperature and larger dew point values
Small CAPE values	Larger CAPE values
Weak CIN	Stronger CIN but ample mid-level instability associated with ERL
Limited vertical wind shear through depth of CBL and above	Frequent upslope component of wind in CBL favours stronger vertical wind shear

It is our hope that the results herein will equip forecasters with a more complete understanding of dryline characteristics in Alberta so that when forecasting or observing drylines an appropriate conceptual model can be applied in the context of the pre-storm environment. Additionally, we hope that these results will aid forecasters in more readily identifying the dryline in coarse operational

‡ Reference to wind shear in Table 4 is with respect to a significant fraction of the lower troposphere as opposed to within or near the CBL. We are not considering low-level wind shear effects on TI though do not discount such influences as discussed in Markowski et al. (2006).

observation networks. The results presented here provide a foundation on which we can improve our understanding of the dryline and TI in Alberta through future research.

ACKNOWLEDGEMENTS

The authors would like to extend gratitude to all field participants and supportive managers and staff at ECCC along with our partners in academia and industry that contributed to a successful field campaign.

REFERENCES

Atkins, N. T., R. M. Wakimoto, and C. L. Ziegler, 1998: Observations of the finescale structure of a dryline during VORTEX 95. *Mon. Wea. Rev.*, **126,** 525–550.

Bluestein, H. B., and T. M. Crawford, 1997: Mesoscale dynamics of the near-dryline environment: Analysis of data from COPS-91. *Mon. Wea. Rev.*, **125,** 2161–2175.

Bluestein, H. B., E. W. McCaul Jr., G. P. Byrd, R. L. Walko, and R. Davies-Jones, 1990: An observational study of splitting convective clouds. *Mon. Wea. Rev.*, **118,** 1359–1370.

Buban, M. S., C. L. Ziegler, E. N. Rasmussen, and Y. P. Richardson, 2007: The dryline on 22 May 2002 during IHOP: Ground-radar and in situ data analyzes of the dryline and boundary layer evolution. *Mon. Wea. Rev.*, **135,** 2473–2505.

Dupilka, M. L., and G. W. Reuter, 2004: A case study of three tornadic storms in Alberta, Canada. Preprint, 22nd Conference on Severe Local Storms, Hyannis, MA. *Amer. Meteor. Soc.*, 3A.6.

Hane, C. E., 2004: Quiescent and synoptically-active drylines: A comparison based upon case studies. *Meteor. Atmos. Phys.*, **86,** 195–211.

Hane, C. E., H. B. Bluestein, T. M. Crawford, M. E. Baldwin, and R. M. Rabin, 1997: Severe thunderstorm development in relation to along-dryline variability: A case study. *Mon. Wea. Rev.*, **125,** 231–251.

Hoch, J. and P. Markowski, 2005: A climatology of springtime dryline position in the U.S. Great Plains Region. *J. Climate,* **18**, 2132–2137.

Knott, S.R.J., and N. M. Taylor, 2000: Operational aspects of the Alberta severe weather outbreak of 29 July 1993. *Natl. Wea. Dig.*, **24:4**, 11-23.

Markowski, P. M., C. Hannon, and E. Rasmussen, 2006: Observations of convection initiation "failure" from the 12 June 2002 IHOP deployment. *Mon. Wea. Rev.*, **134**, 375–405.

Parsons, D., M. A. Shapiro, R. M. Hardesty, R. J. Zamora, and J. M. Intrieri, 1991: The finescale structure of a west Texas dryline. *Mon. Wea. Rev.*, **119,** 1242–1258.

Pietrycha, A. E., and E. N. Rasmussen, 2004: Observations of the dryline: A mobile mesonet perspective. *Wea. Forecasting*, **19**, 1075-1088.

Schultz, D. M., C. C. Weiss, and P. M. Hoffman, 2007: The synoptic regulation of dryline intensity. *Mon. Wea. Rev.*, **135**, 1699–1709.

Sun, W. Y., 1987: Mesoscale convection along the dryline. *J. Atmos. Sci.*, **44,** 1394–1403.

Sun, W. Y., and Y. Ogura, 1979: Boundary layer forcing as a possible trigger to a squall line formation. *J. Atmos. Sci.*, **36,** 235–254.

Taylor, N. M., D. M. L. Sills, J. M. Hanesiak, J. A. Milbrandt, C. D. Smith, G. S. Strong, S. H. Skone, P. J. McCarthy, and J. C. Brimelow, 2010: The Understanding Severe Thunderstorms and Alberta Boundary Layers Experiment (UNSTABLE) 2008. *Bull. Amer. Meteor. Soc.*, **92**, 739-763.

Weiss, C. C., and H. B. Bluestein, 2002: Airborne pseudo-dual Doppler analysis of a dryline–outflow boundary intersection. *Mon. Wea. Rev.*, **130,** 1207–1226.

Weiss, C. C., H. B. Bluestein, and A. L. Pazmany, 2006: Finescale radar observations of the 22 May 2002 dryline during the International H_2O Project (IHOP). *Mon. Wea. Rev.*, **134,** 273–293.

Ziegler, C. L., and C. E. Hane, 1993: An observational study of the dryline. *Mon. Wea. Rev.*, **121,** 1134–1151.

Ziegler, C. L. and E. N. Rasmussen, 1998: The initiation of moist convection at the dryline: Forecasting issues from a case study perspective. *Wea. Forecasting*, **13**, 1106–1131.

Ziegler, C. L., W. J. Martin, R. A. Pielke, and R. L. Walko, 1995: A modeling study of the dryline. *J. Atmos. Sci.*, **52,** 263–285.